EREM 80/2
Journal of Environmental Research, Engineering and Management
Vol. 80 / No. 2 / 2024
pp. 133–143
10.5755/j01.erem.80.2.35188

Investigation of the Relationship between Shaded Cell Temperature and the Operating Point of PV Systems

Received 2023/09 | Accepted after revisions 2024/02

https://doi.org/10.5755/j01.erem.80.2.35188

Investigation of the Relationship between Shaded Cell Temperature and the Operating Point of PV Systems

Zoubeyr Smara[1, 2], Abdelkader Aissat[1, 3]

[1] Laboratory LATSI, University Blida 1, Algeria

[2] Unité de Développement des Equipements Solaires, Algeria

[3] University Ahmed Draia, Algeria

***Corresponding author:** sakre23@yahoo.fr

The building integrated photovoltaic applications (BIPV) are mostly affected by partial shading, which results in a significant decrease in energy efficiency and leads to the apparition of multiple power peaks on the I-V characteristic curve of photovoltaic generators. In mitigating this problem, sophisticated maximum power point tracking techniques (MPPT) are used to track the global peak among the other locals. These techniques do not take into account the overheating of the shaded cells given that, under some critical situations, shaded cell performances may degrade, thus affecting the lifespan of the photovoltaic modules. In this regard, the present work aims to investigate in which peak on the I-V characteristic curve the PV module should operate appropriately with less overheating risk. For that, the shaded cells' temperatures and currents at different operating points were monitored. The results show that the worst-case scenario occurs for small shadow ratios (in the studied case, the shadow ratio 'sr' = 25%) where the temperature of the shaded cell reached approximately three times (300%) the temperature of non-shaded cells. This temperature decreases as the operating point is moved from the short circuit current towards the open-circuit voltage; as a result, the PV module works safely with minimum thermal stress for the maximum power peak near the open-circuit voltage.

Keywords: PV module, cell, thermal stress, overheating, shading, operating point.

Introduction

Nowadays, the growing number of citizens and improving life standards have increased energy consumption in the world (Gecevičius et al., 2021). It is reported that 40% of global energy is consumed by the building sector in several countries (Moran et al.,2017; Amber et al., 2017). The building sector is responsible for

approximately 33% of greenhouse gas emissions (Moran et al., 2017; Coma et al., 2018). In response to these high percentages, the building sector tends towards the application of net zero or nearly zero energy building (ZEB or nZEB, respectively) concept (Longo et al., 2019). In this way, the energy performance of buildings could be improved via the incorporation of renewable energy sources installed on-site or nearby (Aelenei et al., 2019) to satisfy local energy demands (Yang et al., 2019). Photovoltaic energy is one of the most promising renewable sources used to generate electricity in buildings and accelerate the transition towards energy neutral buildings (Spiliotis et al., 2019). However, the BIPV technology is usually affected by shading from surrounding objects (Wendlandt et al., 2010), as seen in the case of the 1000 Photovoltaic Roofs Program executed between 1991 and 1995 in Germany (Jahn et al., 2004). In this program, it was reported that partial shading affects more than 40% of the installed PV systems. Under these adverse conditions, shaded cells become reverse biased, dissipate power in the form of heat, and may cause a hot-spot phenomenon (Satpathy et al., 2017).

In the presence of partial shading, the current-voltage (I-V) characteristic exhibits a multi-step pattern, whereas the power voltage (P-V) characteristic will exhibit a multi-peak pattern (one global maximum and other local maxima) (Malathy et al., 2017). The number of peaks depends upon various factors, such as module interconnection (Patel et al., 2008), shaded area, location of shaded modules within the array, and number of bypass diodes that the PV array contains (Malathy et al., 2015).

In the research literature, the electrical effect of shading on PV modules has been widely investigated. In some studies (Li et al., 2018; Belhachat and Larbes, 2019), reviews of the global maximum power point tracking techniques (GMPPT) using conventional and artificial intelligence concepts have been presented. Some of these techniques were developed, implemented, and then tested through experimental studies (Ahmed et al., 2017). In Batzelis et al. (2015), 46 existing models for partially shaded PV systems were presented. These models were used to describe the PV cell's reverse operation, evaluate shading losses, simulate the I-V curve and determine the global maximum power peaks (GMPPs). To reduce mismatch losses, the partial shading effect on different PV array configurations was studied in (Malathy et al., 2017; Yadav et al., 2017). Some shading fault detection methods were also proposed (Bressan et al., 2016; Fadhel et al., 2019).

On other hand, several works that deal with the thermal effect of shading exist. An experimental study on the hot spot phenomenon is presented in Moretón et al. (2015).In Rossi et al.(2015), a thermal model for the shaded PV modules is proposed. A review on faults and infrared thermography diagnosis was presented in a study by Tsanakas et al. (2016).In other studies(Ma et al., 2019; Gosumbonggot et al., 2019), hotspot detection strategies were discussed. The hot-spot effect on shingled PV modules was investigated in Clement et al. (2020), and the influence of inactive bypass diodes on the temperature distribution in shaded PV modules was studied in Mohammed et al. (2020).

Motivated by the above observations, the work presented in this paper investigates the relationship between the electrical and the thermal behaviors of PV systems under shading conditions. The obtained results showed that the thermal stress undergone by the shaded PV parts depends on the operating point position on the I-V characteristic curve where the temperature decreased as the operating point is moving from the short circuit current towards the open-circuit voltage. This means that the PV module works safely with minimum thermal stress for the maximum power peak near the open circuit voltage.

Problem formulation

Photovoltaic cell modeling

In the research literature, several conventional solar cell models exist. The one- and two-diode models are largely used and referenced (Paraskevadaki et al., 2011). These models are used to obtain the I-V curve and describe the PV cell behavior under irradiation's homogenous distribution. In the presence of shading, negative voltages appear across the affected cells' terminals and thus behave as receivers. Several models have been developed as the previously cited models do not take into consideration the cell reverse operation mode. The alternative models introduce the avalanche

effect in the I-V equation (Alonso-García et al., 2006) where the well-known contributions are those proposed by Bishop (1988), Quaschning et al. (1996), and Alonso-Garcia et al. (2006). However, the most referenced model is that of Bishop, as it reveals good matching with experimental measurements (Piccoli et al., 2019). The Bishop model is represented by *equation (1)*.

$$I = \underbrace{I_{ph} - I_d\left[e^{\frac{q(V+IR_s)}{nkT}} - 1\right] - \frac{V+IR_s}{R_{sh}}}_{forward-bias-range} - \underbrace{a(V+IR_s)\left(1-\frac{V+IR_s}{V_{Br}}\right)^{-m}}_{reverse-bias-range} \quad (1)$$

Where: I_{ph} is the photo-generated current; R_{sh} expresses the shunt resistance; R_s is the series resistance; I_d is the diode's reverse-bias saturation current; n is the diode ideality factor; T is the temperature of the cell; q is the electron charge; k is Boltzman's constant; a (Ω-1) is the fraction of ohmic current involved in avalanche break- down; V_{Br}(V) is the junction breakdown voltage; m is the avalanche breakdown exponent.

The equivalent circuit and the I-V characteristic curves of the Bishop model are shown in *Fig. 1*.

Fig. 1. *(a) Electrical circuit of the Bishop model; (b) I-V curves of the PV cell following the Bishop model*

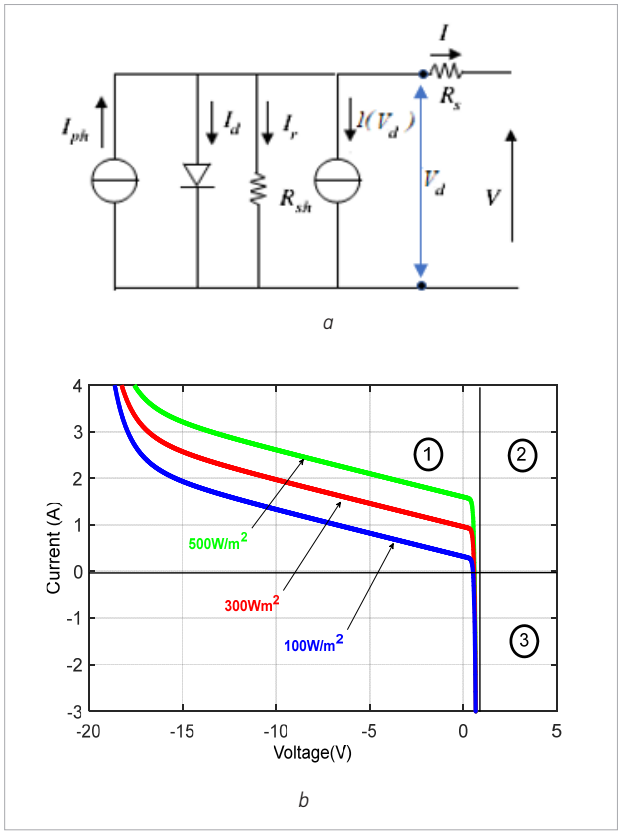

Three operating regions can be distinguished:

Region 1 is characterized by a negative voltage and a positive current. In this region, the PV cell behaves as a receiver. This occurs when the irradiation is not homogeneous on the PV module.

Region 2 is characterized by a positive voltage and a positive current. In this case, the PV cell behaves like a generator. This could be related to homogeneous irradiation on the entire module.

Region 3 is characterized by a positive voltage and a negative current. In this region, the PV module becomes a receiver. This happens in the presence of a directly connected load that can switch from the receiver mode to the generator mode, for example, a battery at night. To avoid this phenomenon, a blocking diode is commonly inserted between the PV generator and the battery.

Fig. 2 shows the experimental I-V and P-V characteristics of a 200 W_p partially shaded module for an irradiance level of 915W/m² and an ambient temperature of 23°C. This module is endowed by three by-pass diodes connected in anti-parallel to three strings of 24 cells. In this test, two partially covered cells named Cell 01 and Cell 02 were considered. The shadow ratio (sr) represents the percentage of the covered part within the cell, where sr = 25% for Cell 01 and sr = 70% for Cell 02. These specific shadow ratios are chosen to have an I-V curve with three steps. The electrical parameters of this module are shown in *Table 1*.

Table 1. *Characteristics of the PV module used in the study*

Module characteristics	Symbol	Numerical value
Maximum power	P_{max}	200 W
Open circuit voltage	V_{oc}	45.6 V
Short circuit current	I_{sc}	5.8 A
Optimal voltage	V_{mp}	36.9 V
Optimal current	I_{mp}	5.42 A
Nominal operating cell temperature	NOCT	45 ± 2
Number of cells	/	72
Number of by-pass diodes	/	03 (01 diode for 24 cells)

To evaluate the two shaded cells' temperature at different operating points, it is necessary to connect the module to a variable load. For this purpose, an Agilent "N3300A

Fig. 2. *(a) Shaded PV module, (b) I-V characteristic curves, (c) P-V characteristic curves*

a

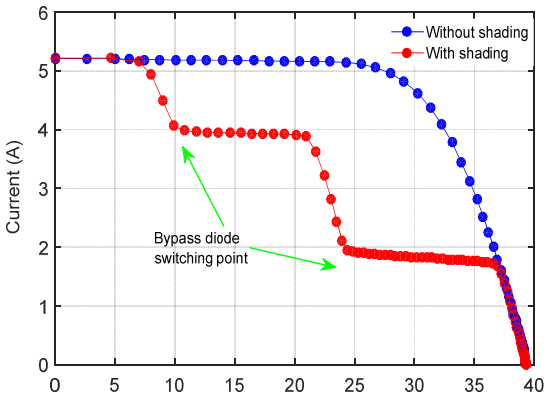

b

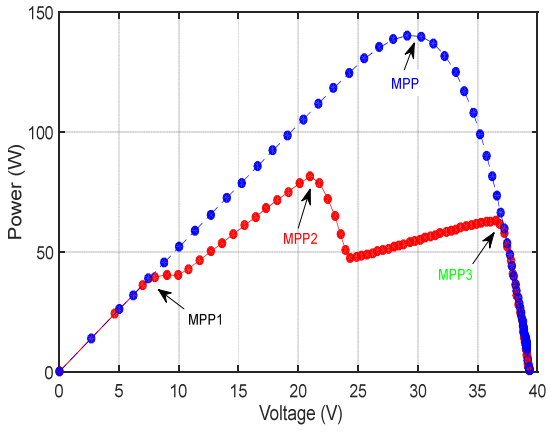

c

1800-Watt DC" Programmable Electronic Load was used. The operating point can be changed by changing the DC electronic load voltage via its LabVIEW interface. The following sections describe the experimental setups used to measure the temperatures and the electrical parameters of the partially shaded module.

Temperature measurement of the shaded cells at different operating points

This setup is used to measure the temperature of the shaded cells and record the module's electrical parameters at different operating points. The setup is depicted in *Fig. 3*. It consists of a PV module (200 W_p) connected directly to the Agilent "N3300A 1800-Watt DC" Electronic Load. Two cells named Cell 01 and Cell 02from different strings of the module were purposely covered with shadow ratios (sr) of 25% and 70%, respectively. Temperatures of the two shaded cells and another unshaded cell were sensed using PT100 sensors placed at the backsides. These sensors were connected to an Agilent data acquisition (34972A) that records and displays measurements in real-time via the LabVIEW interface on a computer. The electronic load could impose different operating voltages during the test period. The voltage, the current, and the power of the module were registered automatically. The sampling rate of the acquisition systems was set to 30 s. The experiments were carried out on a clear day from 12:00 to 14:00. The irradiance 'Φ' varied between 985 W/m^2 and 1025 W/m^2, the ambient temperature 'T' varied between 22.7°C and 23.5°C, and the wind speed 'v' was less than 1 m/s.

The test was divided into eight phases of 15 minutes each (from Ph 01 to Ph 08). In each phase, the electronic load was programmed to impose a specific operating voltage. For the first phase (Ph 01), the electronic load imposed V_{oc} as the operating voltage. For the second Phase (Ph02), the electronic load imposed an operating voltage of 36 volts. Phase after phase, the operating voltages were decreased by 6 V until it reached 06 volts for Phase 07. In the last phase (Ph 08), V_{oc} was imposed again by the electronic load.

Shaded cell performances for any operating point from the I-V curve

This setup is used to calculate the dissipated power by the shaded cells as a function of the module operating voltage. For this purpose, the same partially

Fig. 3. *(a) First setup used for measuring temperatures of the shaded cells and the electrical parameters of the module at different operating points, (b) Bloc diagram of the first setup*

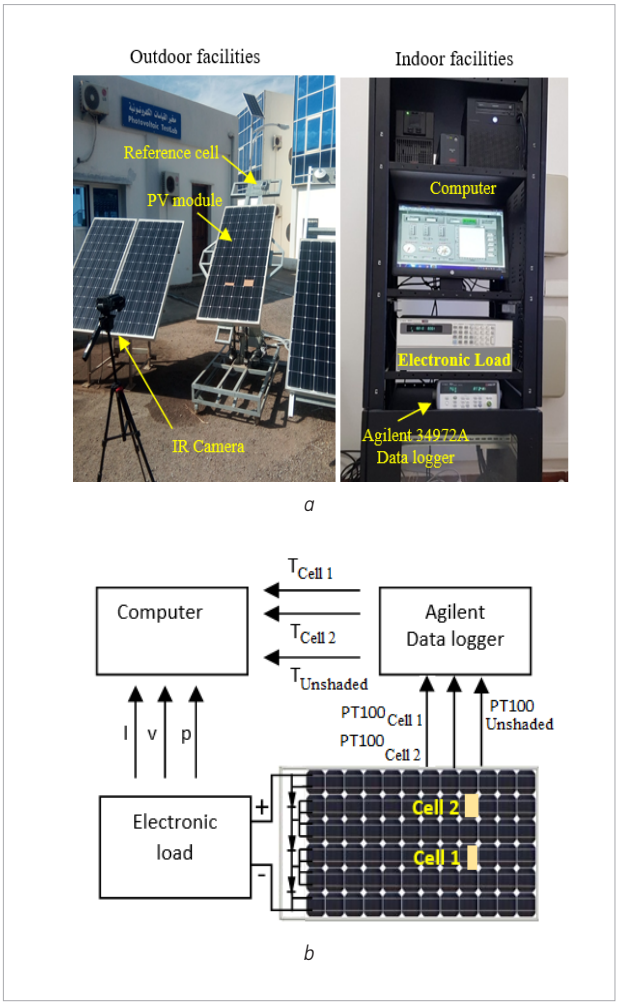

shaded module was connected to an I-V tracer. The idea is to measure the current flows through the shaded cells when the I-V curve is being plotted and then calculating the dissipated power. As it is difficult to measure these currents directly, some minor changes need to be made in the PV module's junction box. The two bypass diodes connected in anti-parallel to the two strings containing the shaded cells were removed and placed in series with current sensors (in the current sensing circuit). Then, each bypass diode/current sensor couple was wired to the junction box. The total current of the module is the current flowing through the unshaded string and can thus be sensed directly. After measuring the current flow through the shaded cells, the dissipated power for any operating point can be calculated easily. A DC power supply was used to feed the current sensors, and a Tektronix oscilloscope was used to measure the current flow through the bypass diodes. The current flow through each string can be computed by using the mathematical function of the oscilloscope.

The setup is depicted in *Fig. 4(a)* and described by the block diagram in *Fig. 4(b)*.

Fig. 4. *(a) Second setup used for measuring shaded cells currents, (b) Bloc diagram of the shaded cells current sensing setup*

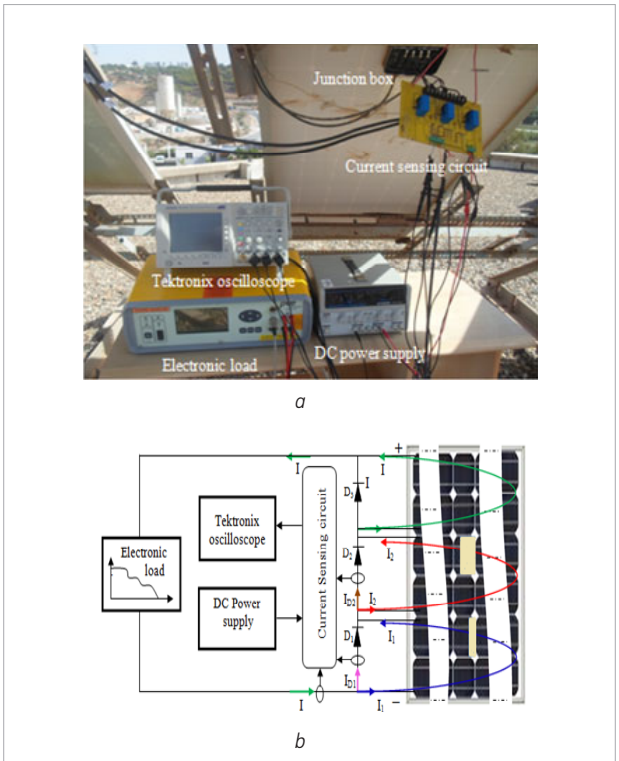

Results and Discussion

The obtained results from the experiment are presented in this section. The variation in the temperature of the shaded cells, output voltage, current, and power are evaluated in the first subsection, while the dissipated power by the shaded cells and their voltages for any operating point are evaluated in the second subsection.

Temperature of shaded cells and electrical output performances of the PV module

For the first setup, the electrical variables, namely current, voltage, and power delivered by the PV module for

the eight operating phases were recorded via an electronic load (Agilent "N3300A 1800-Watt DC"). In contrast, the temperatures of the two shaded cells and the unshaded one were recorded via the data logger (Agilent 34972A). The obtained results are presented in *Fig. 5*.

Fig. 5. *(a) Current, voltage and power of the PV module during the test, (b) Temperatures of the shaded cells during the test*

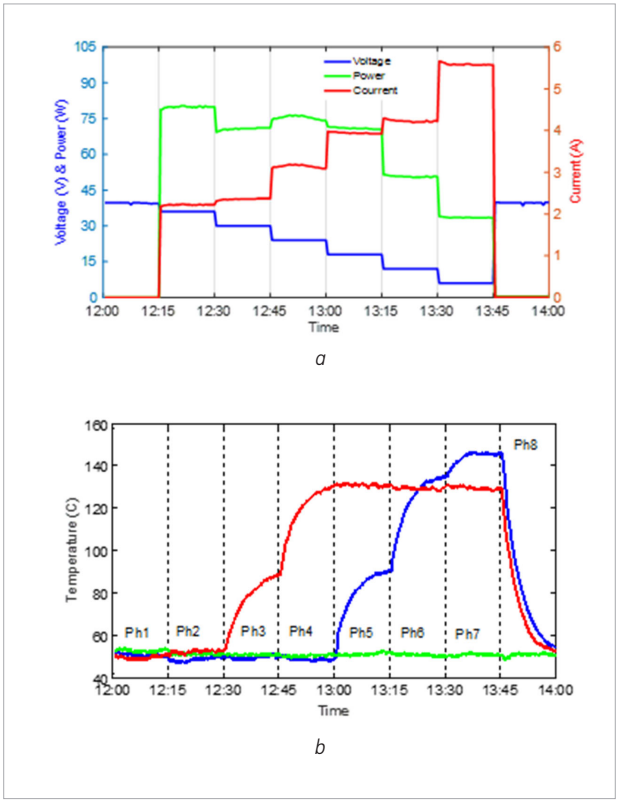

It can be noticed that from Phase 01 to Phase 04, which corresponds to operating voltages of V_{oc}, 36 V, 30 V, and 24 V accordingly, the temperature of Cell 01 (sr = 25%) is steady around 49°C. Starting from Phase 05, with the corresponding operating voltage of 18 V, the temperature for Cell 01 begins to increase until it reaches approximately 90°C. For Phase 06, corresponding to an operating voltage of 12 V, the temperature reaches a high value, which is around 134°C. For Phase 07, which corresponds to an operating voltage of 06 V, the temperature continues to increase until it reaches a maximum value of approximately 145°C. For the last phase (Phase 08), which corresponds to the disconnection of the PV module, the temperature decreases until it reaches the temperature of the surrounding unshaded cells.

For Cell 02 (sr = 70%), the temperature is steady at around 50°C for the first two phases. For Phase 03, however, temperature increases until it reaches 88°C. Furthermore, in Phase 04, the temperature continues to increase until it reaches 130°C and remains steady around this value for Phase 05, 06, and 07. For the last phase (Phase 08), the temperature decreases until it reaches the temperature of the surrounding unshaded cells.

By combining part (a) and (b) of *Fig. 5*, the following noteworthy observations can be made:

Phase 02 (V_2 = 36V) represents the best case with a temperature of approximately 49°C for the two shaded cells and a generated power of 80W.

Phase 07 (V_7 = 06V) represents the worst-case with a temperature of approximately 145°C for Cell 01 (sr = 25%) and 130°C for Cell 02 (sr = 70%) and a generated power of 33W.

Phase 03 and Phase 05 (V_3 = 30V and V_5 = 18V) have approximately a similar generated power (about 70W), but the temperatures of the shaded cells are different (Phase 05 is more stressful than Phase 03).

Table 2 summarizes these significant cases (values were taken at the corresponding phase's end time).

For the worst-case presented by Phase 07, an infrared camera was used to show the temperature distribution

Table 2. *Temperatures of the shaded and unshaded cells for different operating points*

Case	Phase	PV module power (W)	Unshaded cell temperature(°C)	Cell 1 temperature (°C)	Cell 2 temperature (°C)
Generated power (Best case)	Phase 2	80	50	49	51
Generated power (Worst case)	Phase 7	33	49	145	130
Similar generated power	Phase 3	70	51	50	88
	Phase 5	70	50	90	131

in the PV module after achieving thermal equilibrium (at the phase's end time). The resulting image is presented in *Fig. 6*. The intensity towards the yellow color would indicate that the temperature is getting higher.

Fig. 6. *Temperature distribution for the worst case (Phase 7)*

Shaded cells performances for any operating point from the I-V curve

To explain why the temperatures of the shaded cells reached high levels, the second setup was used separately to measure the total current of the module and the current flow through the bypass diodes when the I-V curve was plotted. *Fig. 7* shows the obtained results at an irradiance level of 915 W/m² and an ambient temperature of 23°C. The current flow through the strings can be calculated using the mathematical function of the oscilloscope (string current (I1 or I2) = total current (I) – bypass diode current (ID1 or ID2)).

Fig. 7. *Total current, by-pass diode currents and shaded cells currents when the I-V curve is being plotted*

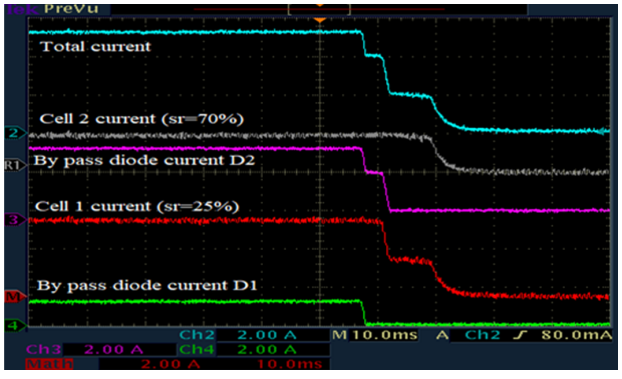

From *Fig. 7*, the current of each shaded cell equals to the total current when the corresponding bypass diode is inactive; it keeps the same current value of the switching bypass diode point when this later is activated (approximately 2 A for Cell 02 and 4 A for Cell 01). *Fig. 8* shows the currents flowing through the shaded cells and the total current versus the module voltage.

Fig. 8. *Current flows through the shaded cells and the non-shaded string versus the module voltage*

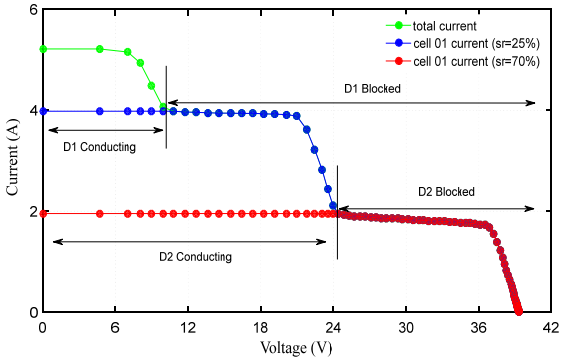

By considering ideal bypass diodes, each shaded cell's reverse voltage can be calculated approximately from the I-V curve. Therefore, the dissipated power by each shaded cell can also be determined. *Fig. 9* illustrates five operating zones for calculating the reverse voltage and the considered cells' dissipated power.

Fig. 9. *Schematic diagram for calculating shaded cells' voltages and powers*

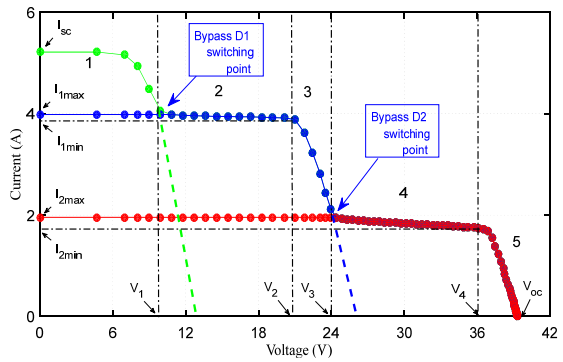

Zone 1 (from 0 to V_1): In this zone, the bypass diode D1 is activated, so the shaded cell 01 voltage and the

voltage of 23 unshaded cells are equal to zero. The voltage of an unshaded cell can be calculated from V_1 (V_1 is the voltage of 24 unshaded cells).

$$V_{Cell\ 01} = -23 * \frac{V1}{24} \quad (2)$$

Zone 2 (from V_1 to V_2): In this zone, the bypass diode D1 is inactive, and the module voltage equals the voltage of the shaded Cell 01 plus the voltage of 47 unshaded cells. By considering that the unshaded cells voltages are constant in this zone, the voltage of the shaded Cell 01 equals the module voltage minus the voltage of 47 unshaded cells.

$$V_{Cell\ 01} = V_{Module} - 47 * \frac{V1}{24} \quad (3)$$

Where: $V_1 < V_{Module} < V_2$

Zone 3 (from V_2 to V_3): In this zone, Cell 01 becomes a generator, and its voltage is identical to the voltage of any other unshaded cell.

$$V_{Cell\ 01} = \frac{V_{Module}}{48} \quad (4)$$

Where: $V_2 < V_{Module} < V_3$

Zone 4 (from V_3 to V_4): In this zone, the bypass diode D2 is blocked, and the module voltage equals the voltage of the shaded Cell 02 plus the voltage of the rest 71 other cells (in this zone, we consider that the voltage of Cell 01 and the other 70 cells are constants).

$$V_{Cell\ 01} = \frac{V3}{48} \quad (5)$$

$$V_{Cell\ 02} = V_{Module} - 71 * \frac{V3}{48} \quad (6)$$

Where: $V_3 < V_{Module} < V_4$

The voltage of Cell 02 in the previous zones is constant (zone 1, 2, and 3); it can be calculated from the *equation (6)* by replacing the 'V_{Module}'by the value 'V_3', the *equation (6)* becomes:

$$V_{Cell\ 02} = -23 * \frac{V3}{48} \quad (7)$$

Zone 5 (from V_4 to V_{oc}): In this zone, Cell 02 becomes a generator like Cell 01, and its voltage equals the voltage of any other unshaded cell.

$$V_{Cell\ 01} = V_{Cell\ 02} = \frac{V_{Module}}{72} \quad (8)$$

Where: $V_4 < V_{Module} < V_{oc}$

The dissipated power by each shaded cell can be determined easily by multiplying its voltage and its corresponding current. In *Fig. 11*, both the voltage and dissipated power by each cell are shown.

Fig. 10 explains clearly why the shaded cells have the temperature trends shown in *Fig. 6 (b)*. Cell 01 (sr = 25%) behaves as a generator when the corresponding bypass diode is switching 'OFF' (the operating point is located in the interval [V_2-V_{oc}]); the reason its temperature stays steady for the first four phases. For the remaining phases within the interval [V_1–V_2], the bypass diode is always switching 'OFF'. Hence, Cell 01 behaves as a receiver and has a negative voltage and dissipates power in the form of heat.

Fig. 10. *The voltage and the dissipated power by each shaded cell versus the I-V curve*

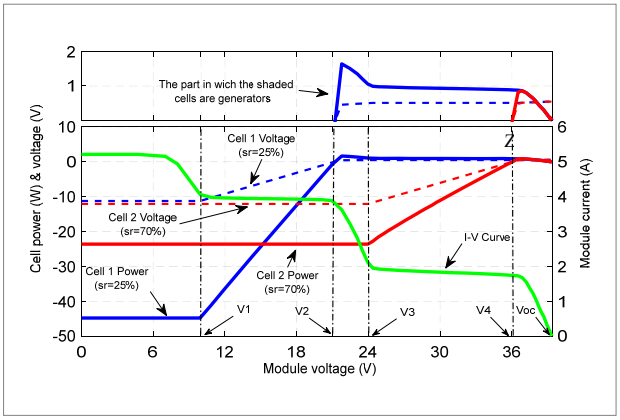

This dissipated power reaches a maximum value when the bypass diode is switching 'ON', and it keeps this value in the interval [0 – V_1]; that is why the Cell 01 temperature reached a high level in Phase 07. Essentially, Cell 02 (sr = 70%) behaves similarly to Cell 01; it becomes a generator when the corresponding bypass diode is switched 'OFF' (in the interval [V_4 -V_{oc}]), which is explained by its steady temperature for Phase 01 and Phase 02. Starting from Phase 03, however, Cell 02 behaves as a receiver.

In Phase 04, the cell dissipates more power until it reaches a maximum value that corresponds to the maximum current flowing through it, specified by its steady temperature from Phase 04 to Phase 07.

In summary, for the nearest maximum power point to V_{oc}, all shaded cells would behave as generators. This point is determined to be the safest operating point for a

PV module and/or array. On the other hand, the highest internal temperature within the shaded cells corresponds to the nearest maximum power point to I_{sc}. This temperature increases when the shadow ratio decreases.

Conclusion

Experimental analyses of the relation between the operating point of a partially shaded PV module and the thermal stress within its shaded parts have been carried out. It was found that this thermal stress is directly proportional to the power dissipated by the shaded parts. The worst-case scenario occurs when the bypass diodes are activated, in which the cell that has the smallest shadow ratio exhibits maximum internal temperature. This temperature is gradually decreasing. When the operating point moves from the diode switching point to the V_{oc} point, both the current and amplitude of the reverse voltage of the shaded cells will decrease. This leads to a decrease in the power dissipated by the shaded cells. When the voltage across the shaded cells becomes positive, the cells will operate as a generator, and its internal temperature will be approximately the same as that of a non-shaded cell. Therefore, the higher the operating point current, the higher the thermal stress within module shaded parts.

Besides, it is worth noticing the following:

- The nearest power peak to the V_{oc} point is the safest peak for the PV module's operation because all shaded cells would behave as generators.
- The nearest power peak to the I_{sc} point is the worst peak for the PV module's operation due to a higher power dissipation by the shaded cells.
- The shaded cells dissipate maximum power when the bypass diode is activated. This dissipated power increases when the shadow ratio of the cell decreases.

Under some partial shading patterns, the peaks that appear on the I-V curve may be equal. In such a case, the MPPT techniques devised to tackle the shading issue may track the peak where the temperature of the shaded cells is higher, which may have adverse effects on the cell performances. The present work results may contribute towards improving the MPPT techniques under partial shading conditions in terms of security against the hot-spot phenomenon. This can be achieved by adding some snippets in the MPPT code to choose the peak where the temperature of the shaded parts is the lowest.

References

Aelenei D. et al., (2019) Investigating the potential for energy flexibility in an office building with a vertical BIPV and a PV roof system. Renewable Energy 137: 189-197. https://doi.org/10.1016/j.renene.2018.07.140

Ahmed J., Salam Z. (2017) An Accurate Method for MPPT to Detect the Partial Shading Occurrence in PV System. IEEE Transactions on Industrial Informatics 83(5): 2151-2161. https://doi.org/10.1109/TII.2017.2703079

Alonso-García M. C., Ruiz J. M. (2006) ,Analysis and modelling the reverse characteristic of photovoltaic cells'.Solar Energy Materials and Solar Cells 90(7-8):1105-1120. https://doi.org/10.1016/j.solmat.2005.06.006

Alonso-García M. C., Ruiz, J. M. and Chenlo F. (2006) Experimental study of mismatch and shading effects in the I-V characteristic of a photovoltaic module. Solar Energy Materials and Solar Cells 90(3): 329-340. https://doi.org/10.1016/j.solmat.2005.04.022

Amber K. P. et al., (2017) Energy Consumption Forecasting for University Sector Buildings. Energies 10(10): 1579. https://doi.org/10.3390/en10101579

Batzelis E. I., Georgilakis P. S. and Papathanassiou S. A. (2015) Energy models for photovoltaic systems under partial shading conditions: a comprehensive review. IET Renewable Power Generation 9(4): 340-349. https://doi.org/10.1049/iet-rpg.2014.0207

Belhachat F., and Larbes C. (2019) Comprehensive review on global maximum power point tracking techniques for PV systems subjected to partial shading conditions. Solar Energy 183: 476-500. https://doi.org/10.1016/j.solener.2019.03.045

Bishop J. W. (1988) Computer simulation of the effects of electrical mismatches in photovoltaic cell interconnection circuits. Solar Cells 25(1): 73-89. https://doi.org/10.1016/0379-6787(88)90059-2

Bressan M. et al., (2016) A shadow fault detection method based on the standard error analysis of I-V curves. Renewable Energy 99: 1181-1190. https://doi.org/10.1016/j.renene.2016.08.028

Clement C. E. et al., (2020) Hotspot development and shading response of shingled PV modules. Solar Energy 207: 729-735. https://doi.org/10.1016/j.solener.2020.06.078

Coma J., Pérez G. and Cabeza L. F. (2018) Green roofs to enhance the thermal performance of buildings and outdoor comfort. In Nature Based Strategies for Urban and Building Sustainability 109-117. https://doi.org/10.1016/B978-0-12-812150-4.00010-0

Drif M. et al., (2008) A new estimation method of irradiance on

a partially shaded PV generator in grid-connected photovoltaic systems. Renewable Energy 33(9): 2048-2056. https://doi.org/10.1016/j.renene.2007.12.010

Fadhel S. et al., (2019) PV shading fault detection and classi fi cation based on I-V curve using principal component analysis : Application to isolated PV system. Solar Energy 179: 1-10. https://doi.org/10.1016/j.solener.2018.12.048

Ferdyn-Grygierek J., and Grygierek K. (2017) Multi-Variable optimization of building thermal design using genetic algorithms. Energies 10(10): 1-20. https://doi.org/10.3390/en10101570

Gecevičius G., and Kavaliauskas Ž. (2021) Development of Renewable Energy in Lithuania : Experience , State and Trends. Environmental Research, Engineering and Management 77(4): 64-72. https://doi.org/10.5755/j01.erem.77.4.29902

Gosumbonggot J., and Fujita, G. (2019) Global maximum power point tracking under shading condition and hotspot detection algorithms for photovoltaic systems. Energies 12(5): 882. https://doi.org/10.3390/en12050882

Hachana O., Tina G. M., and Hemsas K. E. (2016) PV array fault DiagnosticTechnique for BIPV systems. Energy and Buildings 126: 263-274. https://doi.org/10.1016/j.enbuild.2016.05.031

Jahn U., and Nasse W. (2004) Operational performance of grid-connected PV systems on buildings in Germany. Progress in Photovoltaics: Research and Applications 12(6): 441-448. https://doi.org/10.1002/pip.550

Li G. et al., (2018) Application of bio-inspired algorithms in maximum power point tracking for PV systems under partial shading conditions - A review. Renewable and Sustainable Energy Reviews 81: 840-873. https://doi.org/10.1016/j.rser.2017.08.034

Longo S., Montana F., and Riva Sanseverino E. (2019) A review on optimization and cost-optimal methodologies in low-energy buildings design and environmental considerations. Sustainable Cities and Society 45: 87-104. https://doi.org/10.1016/j.scs.2018.11.027

Ma M. et al., (2019) Rapid diagnosis of hot spot failure of crystalline silicon PV module based on I-V curve. Microelectronics Reliability 100: 113402. https://doi.org/10.1016/j.microrel.2019.113402

Malathy S., and Ramaprabha R. (2015) Comprehensive analysis on the role of array size and configuration on energy yield of photovoltaic systems under shaded conditions. Renewable and Sustainable Energy Reviews 49: 672-679. https://doi.org/10.1016/j.rser.2015.04.165

Malathy S., and Ramaprabha R. (2017) Reconfiguration strategies to extract maximum power from photovoltaic array under partially shaded conditions. Renewable and Sustainable Energy Reviews 81: 2922-2934. https://doi.org/10.1016/j.rser.2017.06.100

Mohammed H., Kumar M. and Gupta R. (2020) Bypass diode effect on temperature distribution in crystalline silicon photovoltaic module under partial shading. Solar Energy 208: 182-194. https://doi.org/10.1016/j.solener.2020.07.087

Mohapatra A. et al., (2017) A review on MPPT techniques of PV system under partial shading condition. Renewable and Sustainable Energy Reviews 80: 854-867. https://doi.org/10.1016/j.rser.2017.05.083

Moran P., Goggins J., and Hajdukiewicz M. (2017) Super-insulate or use renewable technology? Life cycle cost, energy and global warming potential analysis of nearly zero energy buildings (NZEB) in a temperate oceanic climate. Energy and Buildings 139: 590-607. https://doi.org/10.1016/j.enbuild.2017.01.029

Moretón R., Lorenzo E., and Narvarte L. (2015) Experimental observations on hot-spots and derived acceptance/rejection criteria Solar Energy 118: 28-40. https://doi.org/10.1016/j.solener.2015.05.009

Orozco-gutierrez M. L. et al., (2014) A method for simulating large PV arrays that include reverse biased cells. Applied energy123: 157-167. https://doi.org/10.1016/j.apenergy.2014.02.052

Paraskevadaki E. V., and Papathanassiou S. A. (2011) Evaluation of MPP Voltage and Power of mc-Si PV Modules in Partial Shading Conditions. IEEE Transactionson Energy Conversion 26(3): 923-932. https://doi.org/10.1109/TEC.2011.2126021

Patel H., and Agarwal V. (2008) MATLAB-Based Modeling to Study the Effects of Partial Shading on PV Array Characteristics. IEEE Transactions on Energy Conversion 23(1): 302-310. https://doi.org/10.1109/TEC.2007.914308

Piccoli E. et al., (2019) Experimental validation of a model for PV systems under partial shading for building integrated applications. Solar Energy 183: 356-370. https://doi.org/10.1016/j.solener.2019.03.015

Prasanth Ram J., and Rajasekar N. (2017) A new robust, mutated and fast tracking LPSO method for solar PV maximum power point tracking under partial shaded conditions. Applied Energy 201: 45-59. https://doi.org/10.1016/j.apenergy.2017.05.102

Quaschning V., and Hanitsch R. (1996) Numerical simulation of current-voltage characteristics of photovoltaic systems with shaded solar cells. Solar Energy 56(6): 513-520. https://doi.org/10.1016/0038-092X(96)00006-0

Ramli M. A. et al., (2017) A review on maximum power point tracking for photovoltaic systems with and without shading conditions. Renewable and Sustainable Energy Reviews 67: 144-159. https://doi.org/10.1016/j.rser.2016.09.013

Rossi D. et al., (2015) Modeling and detection of hotspot in shaded photovoltaic cells. IEEE Transactions on Very Large Scale Integration (VLSI) Systems. 23(6): 1031-1039. https://doi.org/10.1109/TVLSI.2014.2333064

Satpathy P. R., Sharma R., and Jena S. (2017) A shade dispersion interconnection scheme for partially shaded modules

in a solar PV array network. Energy 139: 350-365. https://doi.org/10.1016/j.energy.2017.07.161

Spiliotis K. et al., (2019) Modeling and validation of a DC / DC power converter for building energy simulations : Application to BIPV systems. Applied Energy 240: 646-665. https://doi.org/10.1016/j.apenergy.2019.02.071

Tsanakas J. A., Ha L., and Buerhop C. (2016) Faults and infrared thermographic diagnosis in operating c-Si photovoltaic modules: A review of research and future challenges. Renewable and Sustainable Energy Reviews 62: 695-709. https://doi.org/10.1016/j.rser.2016.04.079

Wendlandt S. et al., (2010) Hot spot Risk analysis on silicon cell modules. In 25th European Photovoltaic Solar Energy Conference and Exhibition. Valencia, Spain, September 2010, pp. 4002-4006.

Yadav A. S. et al., (2017) Performance enhancement of partially shaded PV array using novel shade dispersion effect on magic-square puzzle configuration. Solar Energy 144: 780-797. https://doi.org/10.1016/j.solener.2017.01.011

Yang X., Zhang S., and Xu W. (2019) Impact of zero energy buildings on medium-to-long term building energy consumption in China. Energy Policy 129: 574-586. https://doi.org/10.1016/j.enpol.2019.02.025